Supplementary Information for

Observation of an anomalous decoherence effect in a quantum bath at room temperature

Pu Huang, Xi Kong, Nan Zhao, Fazhan Shi, Pengfei Wang, Xing Rong,
Ren-Bao Liu, and Jiangfeng Du

Supplementary Figures

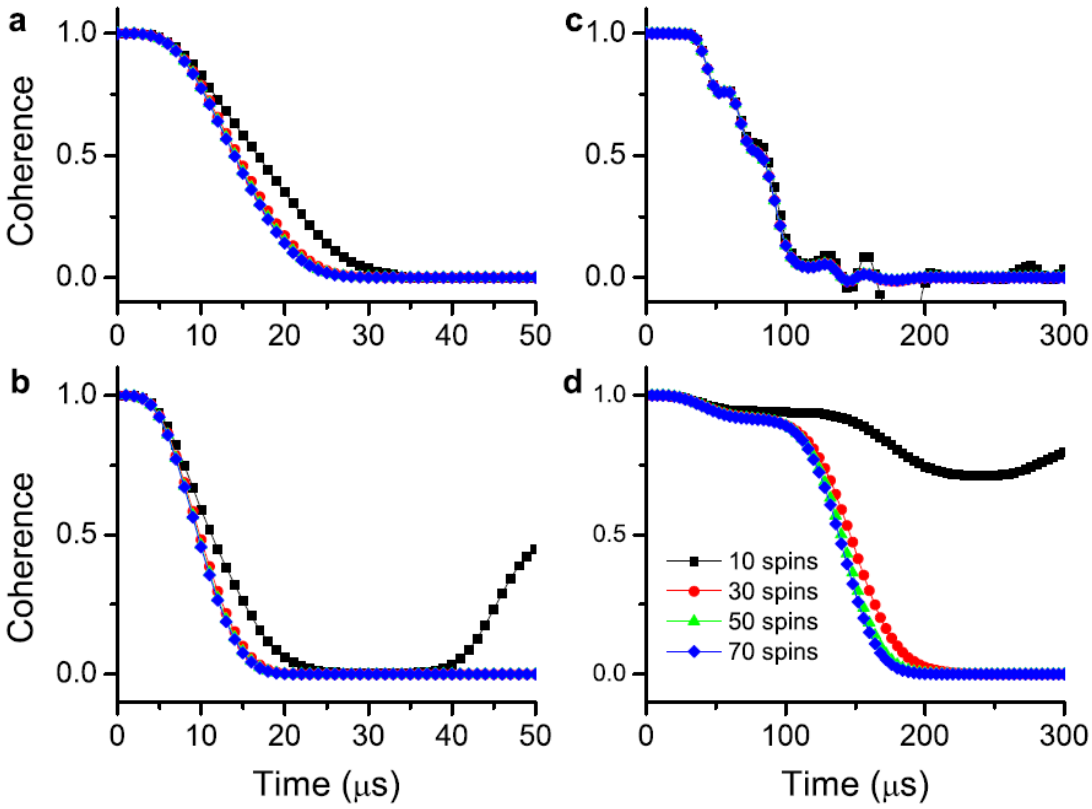

Supplementary Figure S1. Determination of the number of nearest ^{13}C nuclear spins relevant to the centre spin decoherence. **a**, Calculated single-transition coherence of an NV centre spin under the PDD-1 control and a magnetic field B=13.5 Gauss. The numbers of the nearest ^{13}C nuclear spins included in the bath in calculation of different curves are 10 (black line with square symbols), 30 (red line with filled circle symbols), 50 (green line with triangle symbols), and 70 (blue line with diamond symbols). **b**, The same as **a**, but for the double-transition coherence. **c**, The same as **a**, but for the PDD-5 control and the magnetic field 5 Gauss. **d**, The same as **c**, but for the double-transition coherence. For all the cases, the decoherence is mainly caused by the nearest 30 spins.

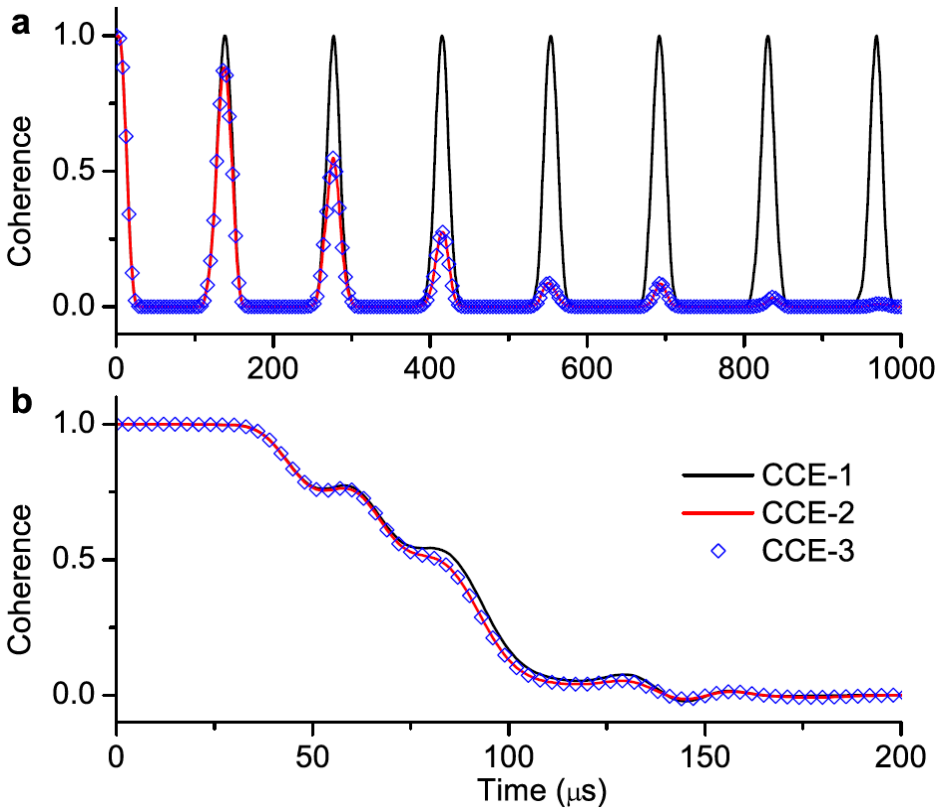

Supplementary Figure S2. Convergence check of the cluster correlation expansion. a, Single-transition coherence $L_{0,+}(t)$ under the Hahn-echo control and a magnetic field B=13.5 Gauss applied along the NV axis, calculated with CCE-1 (black line), CCE-2 (red line), and CCE-3 (blue symbols). **b**, The same as **a** but for the PDD-5 control and the magnetic field B=5 Gauss.

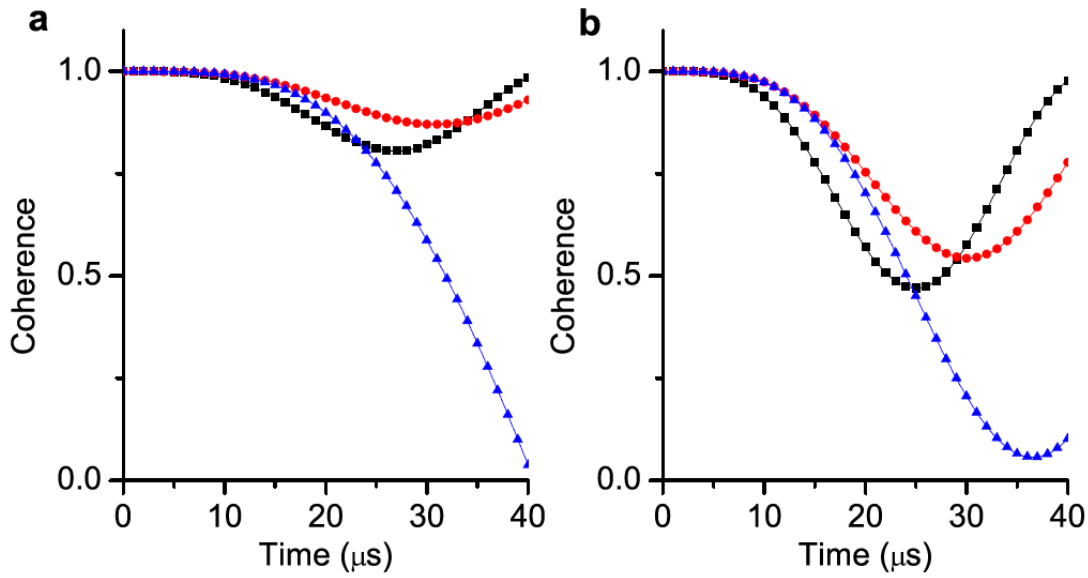

Supplementary Figure S3. Short-time dynamics of single ^{13}C nuclear spins. a, The single-transition decoherence under the PDD-1 (Hahn-echo) control and a 13.5 Gauss magnetic field along the NV axis, individually contributed by three ^{13}C nuclear spins near the centre. **b**, The same as **a**, but for the double-transition. The decoherence is dominated by the short-time dynamics (for the evolution time less than 20 μs).

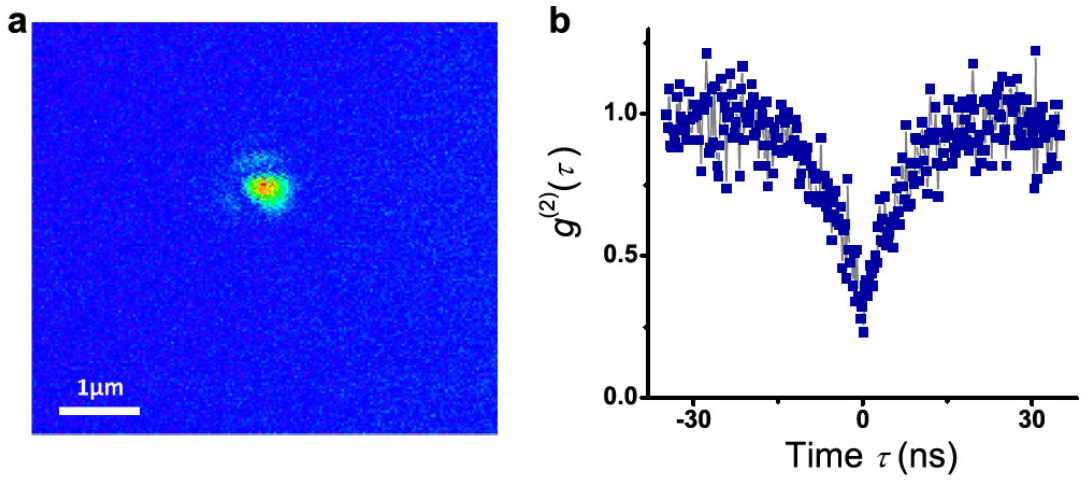

Supplementary Figure S4. Characterization of the single NV centre under study. **a** Scanning confocal image of the NV centre under study (scale bar 1 μm). **b** Fluorescence autocorrelation function of the NV centre. The anti-bunching effect identifies the single NV centre.

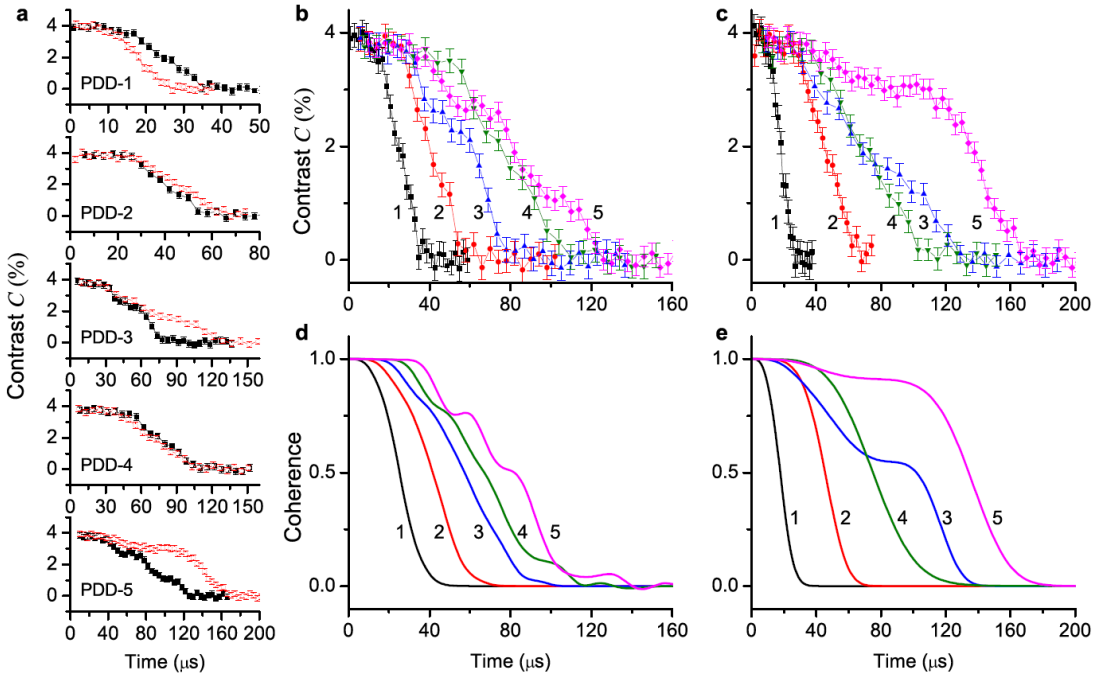

Supplementary Figure S5. Measured contrast of the photon counting of the NV centre under PDD-1 to PDD-5 control. a, Measured contrast of the photon counting (without normalization) for the centre spin single-transition coherence (black) and double-transition coherence (red) under PDD-1 to PDD-5 control (from top to bottom). The experimental conditions are the same as in Figure 4 of the main text. **b** & **c** summarize the experimental results for the single- and double-transition coherence under PDD control (integers indicating the numbers of control pulses), respectively. **d** & **e** are the numerical results.

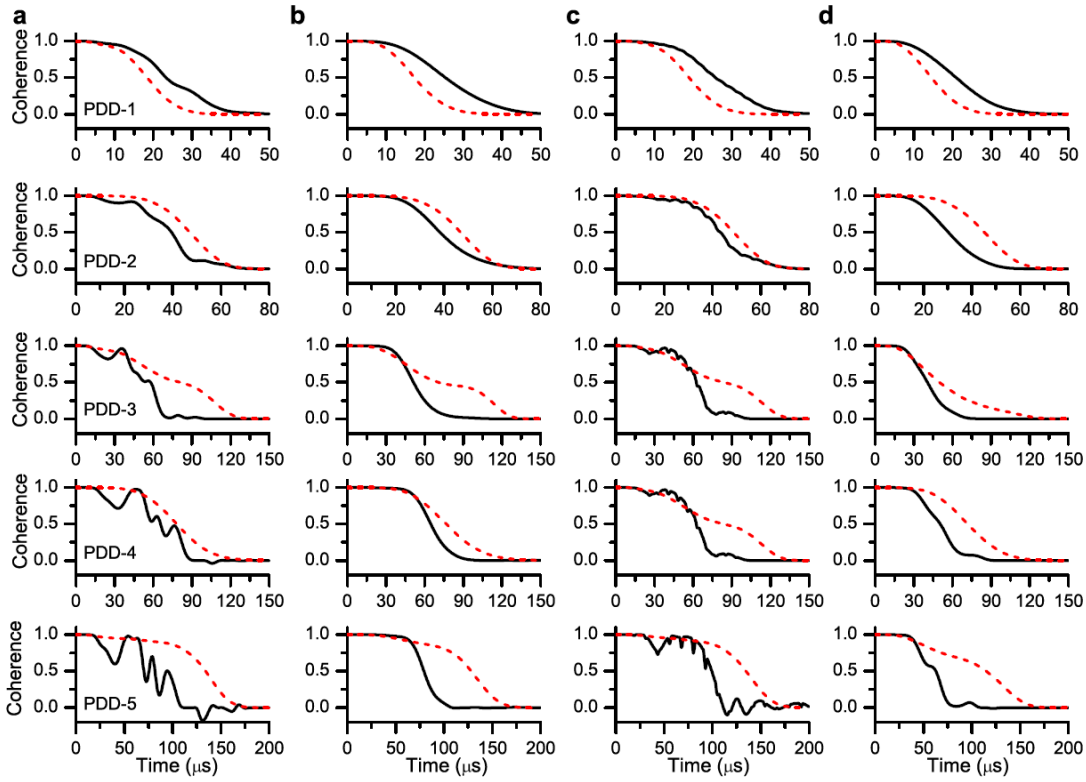

Supplementary Figure S6. Anomalous decoherence effect in baths with different ^{13}C position configurations. a, Calculated single-transition coherence (black solid line) and double-transition coherence (red dashed line) of an NV centre spin under PDD-1 to PDD-5 control (from top to bottom) for a randomly generated ^{13}C nuclear spin bath. **b** – **d**, the same as **a**, but for different ^{13}C position configurations. All the four ^{13}C nuclear spin baths are chosen such that they produce decoherence time T_2 (for the single-transition coherence in Hahn echo) close to the experiment observed value. A magnetic field B=5 Gauss is applied along the NV axis.

Supplementary Notes

Supplementary Note 1. Microscopic model

The system of an NV centre in a nuclear spin bath in high-purity (type IIa) diamond is modeled by the following Hamiltonian

$$H = \Delta S_z^2 + \left(\hat{\mathbf{b}} - \gamma_e \mathbf{B}\right)\cdot \mathbf{S} + H_{\mathrm{B}}, \tag{S1}$$

where Δ is the zero-field splitting of the NV centre spin, γ_e is the electron spin gyromagnetic ratio, $\mathbf{B}$ is the external magnetic field, $\hat{\mathbf{b}}$ is the fluctuating local magnetic field due to hyperfine coupling to the nuclear spins, and H_{B} is the interaction and Zeeman energy of the nuclear spins. The hyperfine coupling to the nuclear spins is

$$\hat{\mathbf{b}} = \sum_j \vec{\vec{\mathbf{A}}}_j \cdot \mathbf{I}_j, \tag{S2}$$

where $\mathbf{I}_0$ is the spin-1 of the host ^{14}N nucleus, $\mathbf{I}_j$ for $j>0$ is the spin-1/2 of the ^{13}C nucleus at $\mathbf{R}_j$ and $\vec{\vec{\mathbf{A}}}_j$ is the hyperfine coupling tensor for the jth nuclear spin. For the magnetic field applied along the NV axis, the bath Hamiltonian H_{B} is

$$\begin{aligned} H_{\mathrm{B}} &= -\sum_j \gamma_j B I_j^z + \Delta_N \left(I_0^z\right)^2 + \sum_{i>j} \frac{\mu_0}{4\pi} \frac{\gamma_i \gamma_j}{R_{ij}^3} \left[\mathbf{I}_i \cdot \mathbf{I}_j - \frac{3\left(\mathbf{I}_i \cdot \mathbf{R}_{ij}\right)\left(\mathbf{R}_{ij} \cdot \mathbf{I}_j\right)}{R_{ij}^2} \right] \\ &\equiv \sum_j \omega_j I_j^z + \sum_{i,j} \mathbf{I}_i \cdot \vec{\vec{\mathbf{D}}} \cdot \mathbf{I}_j, \end{aligned} \tag{S3}$$

where $\gamma_0=\gamma_{\mathrm{N}}=1.93\times10^7\ \mathrm{s^{-1}T^{-1}}$ is the gyromagnetic ratio of the ^{14}N nucleus, $\gamma_{j>0}=\gamma_{\mathrm{C}}=6.73\times10^7\ \mathrm{s^{-1}T^{-1}}$ is that of ^{13}C nuclei, $\mathbf{R}_{ij}=\mathbf{R}_i-\mathbf{R}_j$ is the displacement between the ith and the jth nuclear spins, and $\Delta_{\mathrm{N}}=-5.1$ MHz is the ^{14}N nuclear spin quadrupole splitting [50]. Under a magnetic field applied along the NV axis, the ^{14}N nuclear spin is quantized along the NV axis, which induces a quasi-static frequency shift of the electron spin. The different quasi-static frequency shifts corresponding to the three different spin states of ^{14}N lead to the oscillation in the free-induction decay (FID) of the electron spin coherence and the asymmetric decoherence envelopes (as shown in Figure 2 of the main text). These effects are eliminated in the spin-echo experiments.

We consider the pure dephasing case, since the noise has too small amplitudes and frequencies (as compared with the centre spin splitting Δ) to flip the centre spin, and only the longitudinal component $\hat{b}_z$ of the fluctuating field is relevant. The pure dephasing Hamiltonian is written in a block diagonalized form for different electron spin states $|\alpha\rangle$ with α=0, ± as

$$H = \sum_\alpha |\alpha\rangle\langle\alpha| \otimes \left(\omega_\alpha + H^{(\alpha)}\right), \tag{S4}$$

where $\omega_\alpha = \Delta - \alpha\gamma_{\mathrm{e}} B$, and the bath Hamiltonian $H^{(\alpha)}$ conditioned on the centre spin

state is

$$H^{(\alpha)} = H_{\mathrm{B}} + \alpha \sum_i \mathbf{A}_i \cdot \mathbf{I}_i = H_{\mathrm{B}} + \alpha \hat{b}_z, \tag{S5}$$

with $\mathbf{A}_i = \hat{\mathbf{z}} \cdot \vec{\mathbf{A}}_i$ denoting the hyperfine field felt by the *i*th nuclear spin.

Supplementary Note 2. Decoherence due to classical noise

In the high temperature limit ($k_{\mathrm{B}}T >> \hbar\gamma_i B$), the density matrix of the bath is $\rho_{\mathrm{B}} = 2^{-N}\sum_J |J\rangle\langle J|$, where *N* is the number of ^{13}C spins in the bath, and $\{|J\rangle\}$ is an orthogonal complete basis. We can choose $\{|J\rangle\}$ as eigenstates of the Overhauser field $\hat{b}_z$, with $\hat{b}_z|J\rangle = b_J|J\rangle$. The thermal distribution of the nuclear spin states lead to a Gaussian distribution of the Overhauser field (according to the central limit theorem), with a broadening width

$$\Gamma^2 = \langle \hat{b}_z \rangle = \left\langle \sum_i (\mathbf{A}_i \cdot \mathbf{I}_i)^2 \right\rangle = \frac{1}{4}\sum_i A_i^2. \tag{S6}$$

The FID is caused by this inhomogeneous broadening. In the random Overhauser field, the electron spin in the states $|\pm\rangle$ acquires a random phase $\pm\phi(t) = \pm b_J t$ relative to the state $|0\rangle$. The FID of the single-transition coherence is

$$L_{0,+}(t) = \left\langle e^{-i\varphi(t)} \right\rangle = \exp\left(-\Gamma^2 t^2/2\right). \tag{S7}$$

The FID of the double-transition coherence is

$$L_{+,-}(t) = \left\langle e^{-2i\varphi(t)} \right\rangle = \exp\left(-2\Gamma^2 t^2\right) = \left[L_{+,-}(t)\right]^4. \tag{S8}$$

The dephasing time $T_2^* = \sqrt{2}/\Gamma$ and the decoherence time T_2 depend on the random positions of the ^{13}C atoms in the diamond lattice [48]. In the numerical simulation, we randomly chose a configuration of ^{13}C atom positions which produces T_2^* (for single-transition coherence FID) and T_2 (for single-transition coherence Hahn echo) close to the experimental results under 13.5 Gauss field. Different choices of the ^{13}C atom random positions do not affect the essential results, but only introduce differences in the detailed features. This is verified by simulation of NV centre spin single- and double-transition coherence under multi-pulse dynamical decoupling control for several random configurations of ^{13}C atoms (see Supplementary Figure S6).

Supplementary Note 3. Decoherence due to quantum noise

The decoherence of the centre spin due to coupling to the nuclear spin bath is

calculated with the full quantum theory [26]. Since the hyperfine interaction strength decreases rapidly with the distance between the centre and the nuclear spin, only a finite number of nuclear spins within a certain range from the centre are relevant to the centre spin decoherence. In numerical calculation, we have checked various choices of the bath size (see Supplementary Figure S1), and found that inclusion of about 100 ^{13}C nuclear spins within about 2 nm from the centre is sufficient to produce converged results of the centre spin decoherence. Actually, the decoherence is mainly caused by less than 30 nuclear spins near the centre (see Supplementary Figure S1).

With dynamical decoupling control pulses applied at times t_1, t_2, …, the centre spin coherence $L_{\alpha,\alpha'}(t)$ of the transition $|\alpha\rangle \leftrightarrow |\alpha'\rangle$ is given by

$$L_{\alpha,\alpha'}(t) = \mathrm{Tr}\left[\cdots e^{-iH^{(\alpha)}(t_2-t_1)} e^{-iH^{(\alpha')}t_1} e^{iH^{(\alpha)}t_1} e^{iH^{(\alpha')}(t_2-t_1)} \cdots\right]. \tag{S9}$$

In this work, we consider the periodic dynamical decoupling (PDD), in which the pulses are applied at times τ, 3τ, 5τ, …. In the simulation, the microwave pulses that flip the centre spin are approximated as instantaneous since they have durations much less than the centre spin decoherence time. The cluster correlation expansion (CCE) is used to calculate the coherence $L_{\alpha,\alpha'}(t)$ [26]. In this method, the coherence $L_{\alpha,\alpha'}(t)$ is expressed as the product of cluster correlations

$$L_{\alpha,\alpha'}(t) = \prod_C \tilde{L}^{(C)}_{\alpha,\alpha'}(t), \tag{S10}$$

with the irreducible correlation $\tilde{L}^{(C)}_{\alpha,\alpha'}(t)$ of cluster C recursively defined by

$$\tilde{L}^{(C)}_{\alpha,\alpha'}(t) = \frac{L^{(C)}_{\alpha,\alpha'}(t)}{\prod_{C'\subset C} \tilde{L}^{(C')}_{\alpha,\alpha'}(t)}, \tag{S11}$$

where $L^{(C)}_{\alpha,\alpha'}(t)$ is calculated the same as in Supplementary Eq. (S9) but with only interaction within the cluster C included in the bath Hamiltonian. In realistic calculation, the expansion is truncated at a certain size $|C| \le M$ of clusters (denoted by CCE-M). We have checked the convergence of the CCE (see Supplementary Figure S2), and all the numerical results in the paper are converged.

With the CCE method, we can identify the contributions of different physical processes to the centre spin decoherence. Under the weak magnetic field, the initial stage of decoherence is mainly caused by the single nuclear spin dynamics, i.e. CCE-1, as shown in Supplementary Figure S2. The single-transition coherence recovery is suppressed by the interactions between nuclear spins, especially the pairwise dynamics.

To have a better understanding of the centre spin decoherence in the nuclear spin bath under the dynamical decoupling control, we show in Supplementary Figure S3 the centre spin decoherence individually caused by a few closely located nuclear spins

under various dynamical decoupling control. In Hahn echo (PDD-1), the short-time condition is roughly satisfied for most nuclear spins. In this short-time limit, the centre spin decoherence due to the *j*th nuclear spin is

$$\begin{aligned} L_{0,+}^{(j)}(2\tau) &\approx 1-\frac{1}{8}\left|\gamma_{\mathrm{C}}\mathbf{B}\times\mathbf{A}_j\right|^2\tau^4, \\ L_{+,-}^{(j)}(2\tau) &\approx 1-\frac{1}{2}\left|\gamma_{\mathrm{C}}\mathbf{B}\times\mathbf{A}_j\right|^2\tau^4 \approx \left[L_{0,+}^{(j)}(2\tau)\right]^4. \end{aligned} \tag{S12}$$

The single- and double-transition Hahn-echo decoherence induced individually by several nuclear spins is shown in Supplementary Figures S3a and S3b, respectively.

In a time less than 20 μs, the scaling relation predicted by Supplementary Eq. (S12) approximately holds and the single-transition coherence decays slower than the double-transition coherence in Hahn echo (PDD-1). With increasing the number of dynamical decoupling pulses, the electron spin coherence time is prolonged, and the short-time condition is violated. As shown in Figure 5c of the main text, the single-transition coherence under the PDD-5 control exhibits strong oscillations before it vanishes. However, the decay of double-transition coherence is greatly suppressed (see Figure 5d of the main text) due to the anti-parallel of the effective local fields. The farther and relatively weakly coupled ^{13}C spins become more important than in the single-transition coherence [see Supplementary Figure S1].

Supplementary References

50. He, X. F., Manson, N. & Fisk, P. Paramagnetic resonance of photoexcited NV defects in diamond. II. Hyperfine interaction with the N nucleus. *Phys. Rev. B*, 8816-8822 (1993).